Open Access

Catalysis Research

LIDSEN Publishing Inc.

Original Research

Synthesis and Characterization of MCM-41 Nanomaterials Containing Titanium and Application for Catalytic Oxidation of BTEX

Lidiane A. Morais [1], Francisco L. Castro [2], Glauber J. T. Fernandes [2], Marcio D. S. Araujo [2], Mirna F. Farias [3], Ana P.M.A. Guedes [4], Valter J. Fernandes Jr. [2], Antonio S. Araujo [2, *]

1. Federal Rural University of the Semi-arid, Angicos Campus, 59515-000, Angicos RN, Brazil; E-Mail: Lidiane.morais@ufersa.edu.br
2. Federal University of Rio Grande do Norte, Institute of Chemistry, 5978-970, Natal RN, Brazil; E-Mails: dfranciscolaerte@gmail.com; glauberturolla@gmail.com; marcio.ifrn@gmail.com; valter.fernandes@ufrn.br; antonio.araujo@ufrn.br
3. SENAI Institute for Innovation in Renewable Energies (ISI-ER), 59063-400, Natal RN, Brazil; E-Mail: mirna@isi-er.com.br
4. Federal University of Paraiba, Department of Chemistry, 58051-900, Joao Pessoa PB, Brazil; E-Mail: anachemistry@hotmail.com

* **Correspondence:** Antonio S. Araujo; E-Mail: antonio.araujo@ufrn.br

Academic Editor: Narendra Kumar

Special Issue: Nanoparticles and Nanotechnologies in Catalysis

Catalysis Research
2023, volume 3, issue 2
doi:10.21926/cr.2302017

Received: August 17, 2022
Accepted: May 24, 2023
Published: May 30, 2023

Abstract

The TiO_2/MCM-41 nanomaterials were synthesized by impregnation with an excess solvent with different percentages of titanium dioxide. They were used for catalytic degradation of Benzene Toluene Ethylbenzene and Xylenes (BTEX) in the presence of hydrogen peroxide in aqueous media. The obtained materials were characterized by X-ray Diffraction, nitrogen adsorption-desorption using the BET method and Fourier Transform Infrared Spectroscopy. The nanostructured phase of the hexagonal ordered materials was obtained even after modification with titanium oxide and calcination. The characterizations have proven the effectiveness of the synthesis method used to incorporate titanium with anatase structure

impregnated in the nanoporous of the MCM-41 material. Anatase is the main active phase of TiO_2 to oxidize organic compounds. The catalytic evaluation wascarried out in a semi-bath reactor with 20 mL of a mixture containing BTEX (100 µg/L), hydrogen peroxide (2.0 mol/L) and TiO_2/MCM-41 (2.0 g/L) in aqueous media. The reactions were carried out at a temperature of 60°C for 5 hours, and the analyses were performed by gas chromatography with a photoionization detector and headspace sampler. The catalytic tests showed satisfactory results with more than 95% of conversion, where the catalyst 48%TiO_2/MCM-41 presented higher performance.

Keywords
Nano porous materials; MCM-41; titanium oxide; advanced oxidation process; BTEX

1. Introduction

Titanium oxide has been one of the most used materials as catalysts for the oxidation of hydrocarbons due to its photocatalytic properties, in addition to presenting corrosion resistance, and chemical stability and mainly because it is a low-cost material [1, 2]. However, titanium oxide has some limitations related to its low specific surface area and low porosity, which limits its catalytic activity for oxidation and removal of some organic pollutants from the environment [3, 4]. Thus, one of the ways that can be considered to improve its catalytic activity is to obtain TiO_2 composites supported on porous adsorbents of different natures, such as silica [5, 6], zeolites [7, 8] and active carbon [9, 10].

For correct water treatment, in addition to organic pollutants, heavy metals must also be removed. The use of compounds based on high surface area glycidoxypropyltrimethoxysilane decorated magnetic more-aluminosilicate shell $Na(Si_2Al)O_6.xH_2O/NiFe_2O_4$ structures was synthesized and successfully applied to remove the toxic lead and cadmium ions from the waste waters [11]. Pollution by organic compounds in water has been a major environmental concern. One way to reduce this problem is through photocatalysis. Photocatalyst materials based on $Ag/AgCl/ZnTiO_3$ have been active for these pollutant degradation reactions [12]. Silica-based nanostructures containing silver were synthesized by modifying the surface of hexagonal silica nanoparticles and tested as photocatalysts for the degradation of semi-volatile organic compounds (SVOCs), namely 4-methoxy-2-nitrophenol and 3-methyl-4-nitrophenol in the presence of gram-positive bacteria under visible light [13]. Tube-like nanostructures gC_3N_4($T\text{-}C_3N_4$) decorated with Ag/AgCl were fabricated by pyrolysis and coprecipitation methods, and tested as photocatalysts for degradation of Acid Blue 92 (AB92) dye under visible light [14].

New photocatalytic materials based on $Ag@Ag_2MoO_4$/polyoxomolybdate/C_3N_4 were synthesized by the combined method of pyrolysis-coprecipitation at room temperature. These materials showed good photocatalytic performance for removing the coloring compound Anazolone Sodium and for treating biomedical waste [15, 16]. A new quaternary magnetic photocatalyst, $K_4Nb_6O_{17}/\alpha\text{-}Fe_2O_3/Fe_3N/g\text{-}C_3N_4$, was synthesized through a one-step thermal pyrolysis process. The photocatalytic activity was evaluated for acetamiprid pesticide degradation, CO_2 reduction reaction and eradication of U87-MG cells. Due to the presence of several photosensitive compounds, the

obtained photocatalyst showed excellent ability to collect visible light photons, despite its high calculated bandgap of 2.75 eV. With 76% removal efficiency for acetamiprid pesticide degradation after five reaction cycles [17].

The main contaminants of groundwater are monoaromatic hydrocarbons BTEX (Benzene, Toluene, Ethylbenzene and Xylene isomers), present in gasoline and various industrial processes, having high toxicity and solubility in water, so causing a large environmental risk [18-20]. Because of their soluble characteristics, petroleum products's organic chemicals (BTEX) can enter soil and groundwater systems and cause serious pollution problems, therefore, reducing and controlling pollution of these constituents has been challenging for the industry.

Several technologies have been developed to address environmental matrices contaminated with compounds aromatics BTEX; among them are adsorption, condensation, thermal decomposition, catalytic incineration, biofiltration, photocatalytic oxidation and advanced oxidation processes [21, 22]. Among these techniques, we highlight the Advanced Oxidation Processes (AOP´s) which are characterized by the same chemical feature: production of •OH radicals; these processes have the main advantage are rapid reaction rates, the potential to reduce toxicity and possibly complete mineralization of organics treated, does not produce materials that require further treatment [23].

The selection of the catalytic materials for various organic pollutants has been the subject of many studies, where two classes of catalysts, noble metals and transition metal oxides, are the most promising catalysts for AOP's [24, 25]. The performance of metal-supported catalysts for organic molecules pollutants oxidation has been reported to be dependent on many factors, such as the nature and properties of the support, metal loading, metal size, preparation method and the pretreatment conditions of the catalysts and the nature and concentration of the organic molecule to be oxidized.

In 1992 researchers at Mobil Oil Corporation discovered the M41S family of mesoporous silicates [26]. Among this family's silicates is the MCM-41 (Mesoporous Composition of Matter), which is characterized by an array ordered hexagonal mesoporous, high surface area and pore diameters of 2-10 nm [27]. However, for these materials to be used as catalysts for advanced oxidation processes, the transition metals are incorporated into the structure for generating the active sites [28, 29]. Titanium has attracted great attention for the catalytic oxidation of various organic substrates and in preparing materials with high catalytic activity [30-33].

Thus, this study aimed to evaluate the catalytic activity of MCM-41 nanostructured material supported with different percentages of titanium dioxide for application in the removal of BTEX aromatic compounds in the presence of hydrogen peroxide in aqueous media. The nanoparticles of TiO_2 can penetrate inside the pores of the support, enabling the immobilization of nano-scaled TiO_2 to develop a catalyst with high performance for the oxidation of organic compounds.

2. Materials and Methods

2.1 Synthesis of MCM-41 and TiO_2/MCM-41

The MCM-41 molecular sieve was synthesized by hydrothermal method with the procedure previously reported [34], using sodium silicate, silica gel, sodium hydroxide and cetyltrimethylammonium as an organic template. The titanium oxide catalyst supported in the MCM-41 was prepared by the post-synthesis method using isopropanol as a solvent in excess. For

this procedure, 1.0 g of calcined MCM-41 and titanium trichloride in 15% HCl (Merck) were physically mixed in quantities necessary for obtaining approximately 30 and 50% by weight of titanium dioxide. The materials were submitted to stirring at room temperature and heating at 100°C until complete evaporation of the solvent and dried in an oven at 100°C for additional 4 hours. Then, the materials were calcined at 550°C for 2 h under an air atmosphere.

2.2 Materials Characterization

The chemical compositions of the MCM-41 and titanium oxide were determined from X-ray Fluorescence dispersive energy (XRF) using a Shimadzu equipment model EDX-800. The XRF spectra were obtained using approximately 50 mg of sample in fine powder introduced in polyethylene holders that present low X-ray absorption in the range studied.

The crystallographic properties of the materials were characterized by X-ray Diffraction in the Rigaku Miniflex II equipment using CuKα radiation (30 kV and 30 mA), in low 2θ angle, 1 to 10 degree, for the characterization of MCM-41 material, and at 2θ from 10 to 80 degree, for determination of TiO_2 crystalline phase. The average particle size was calculated using the Scherrer equation:

$$d_{(hkl)} = \frac{k\lambda}{\beta \cos \theta} \quad (1)$$

where, $d_{(hkl)}$ is the average crystallite size, k is the Scherrer's constant (0.89), λ is the wavelength predominant X-rays (Cu-Kα radiation, λ = 0.1541 nm), β is the width at half height of the diffraction peak (in radians) and θ is the Bragg diffraction angle. The value of "d" was determined for the crystallographic direction (101), equivalent to the highest intensity XRD peak, observed at 25.3°. The absorption spectra in the Fourier Transform Infrared (FTIR) were obtained in the range of 400-4000 cm^{-1} with a resolution of 4 cm^{-1} and 32 scans using a Thermo Nicolet equipment Nexus 470 model.

The nitrogen adsorption/desorption isotherms at 77 K, were performed using a Quanta chrome equipment Nova 1200e model, where the samples were degassed at 300°C for 3 hours under vacuum in a relative pressure (P/P_0) ranging from 0.05 to 0.95. The specific surface area was determined using the BET method, and data relating to volume and pore diameter were used by mathematical models by the BJH method.

2.3 Catalytic Evaluation

The reactions were performed in glass microreactors of 20 mL and vials closed using Teflon septum. For the reactions, solutions containing 100 μg L^{-1} of BTEX patterns were prepared in Milli-Q water, 0.1 mol L^{-1} of H_2O_2 solution and 2.0 g L^{-1} of titanium-based catalysts at pH = 3.0 (HCl solution). The solutions were submitted to a thermostatic bath at 60°C for 5 hours. The catalytic activity of the materials for BTEX removal was performed every hour through the analysis of the products, using a gas chromatograph with photoionization and flame ionization detection (GC-PID/FID), with auto samples by static headspace Triplus model (85°C) Thermo Scientific, trace GC Ultra model, equipped with a column CP-select 624 CB 75 m × 0.53 mm × 3 μm, with a constant flow of helium at 8.0 mL mim^{-1}. Thus, each organic compound's concentration (% volume) was determined as a function of reaction time.

3. Results and Discussion

3.1 Characterization of the Catalysts

The chemical composition of the calcined materials, as determined from XRF, proved that the samples presented the following concentrations: 31%TiO_2/MCM-41 and 48%TiO_2/MCM-41, evidencing the efficiency of the impregnation method used. The X-ray Diffraction patterns of the mesoporous MCM-41 support and TiO_2/MCM-41 catalysts with different percentages of titanium in low and high angles are shown in Figure 1.

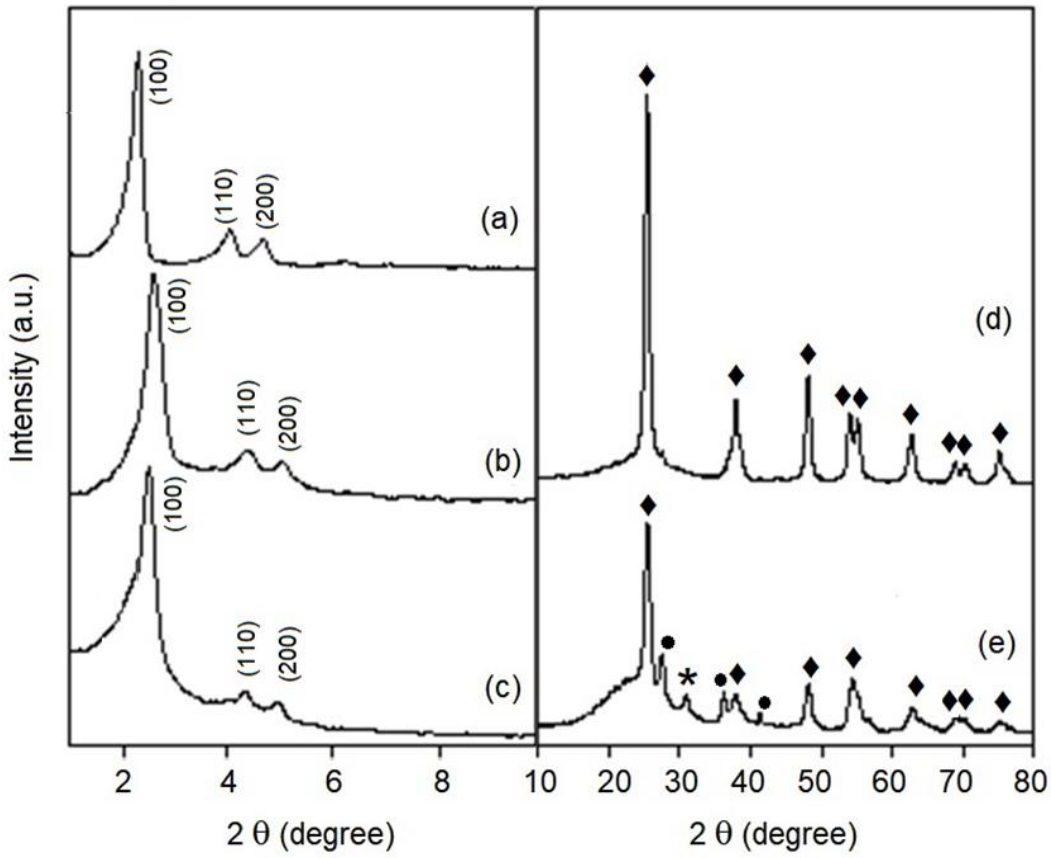

Figure 1 XRD patterns of mesoporous materials: (a) MCM-41; (b) 31%TiO_2/MCM-41; (c) 48% TiO_2/MCM-41 in low angle; (d) 31%TiO_2/MCM-41; (e) 48%TiO_2/MCM-41. (♦ = Anatase; ● = Rutile and * = Bruckite) in high angle.

As observed in Figure 1, high quality of MCM-41 material was obtained, due the presence of three main reflection peaks, related to the planes whose Miller indices are (100) (110) and (200), which are characteristic of materials with well-ordered hexagonal array [35-37]. For the catalysts impregnated with titanium oxide, these planes were observed indicating that the impregnation of titanium was successfully performed without destruction of the structure of the MCM-41 support. One shift of the reflection index (100) for the modified material was attributed to the incorporation of titanium in the structure of silica was observed.

From XRD data obtained at high angle region (2θ 10 to 80 degrees), with the aid of the database JCPDS-ICDD (International Centre for Diffraction Data – Joint Committee on Powder Diffraction

Standards), it was possible to identify the anatase crystalline single phase of titanium dioxide in the 31%TiO_2/MCM-41 sample. For the 48%TiO_2/MCM-41 sample, the rutile and brucite phases were observed, jointly with the single and stable anatase phase, decreasing consequently the pore size of the catalyst. These data are consistent with the literature [38, 39]. The presence of strong peaks at 25.3°, 37.8° and 47.9° proved that the anatase phase is predominant, the photoactive phase for catalysis, as recently reported [40]. Titanium oxide has some limitations related to its low specific surface area and low porosity, which limits its catalytic activity for oxidation. To improve its dispersion, it was used values considered high. According to the Scherrer equation, the particle diameter related to a more intense peak, at 25.3° $d_{(101)}$ was ca. 11.5 nm for 31%TiO_2/MCM-41 and 13.4 nm to 48%TiO_2/MCM-41, evidencing that part of TiO_2 was impregnated in the external pore of the MCM-41. A decrease in the pore diameter of the TiO_2/MCM-41 material was observed, so it was suggested that part of the TiO_2 particles would be impregnated at the entrance of the pores of the MCM-41, as observed in Figure 2.

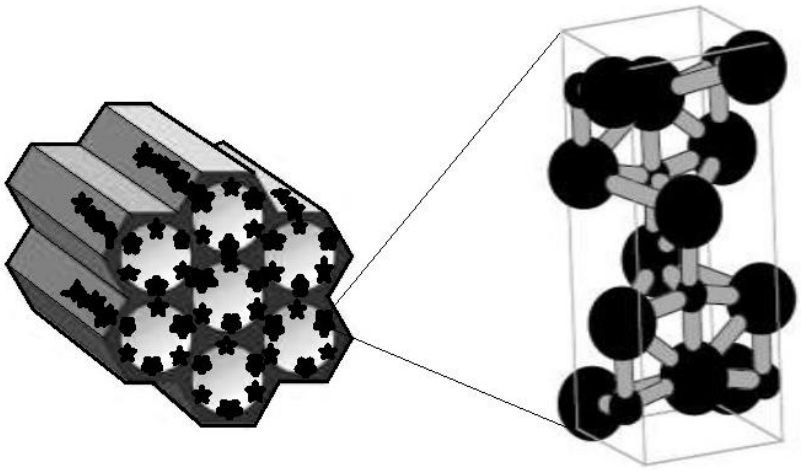

Figure 2 Proposed nanostructuted MCM-41 containing titanium oxide showing a detail of the Anatase active phase of the TiO_2 inside the pores of the hexagonally ordered nanomaterial, as well as crystallite outside of the pores.

The nanoparticles of TiO_2 supported in MCM-41 increased the hydrothermal stability of the material being an important material for catalytic applications. This stability is due to the effect caused by the surface/volume ratio, producing an excess of atoms on the MCM-41 about its expanded volume and surface area, consequently decreasing the energy required for physicochemical transformations.

The nitrogen adsorption-desorption isotherms were obtained at 77 K for the MCM-41 and TiO_2/MCM-41 catalysts are shown in Figure 3. The materials presented type IV isotherms containing hysteresis, characteristic of mesoporous materials with uniform systems of cylindrical pores, according to the classification of the IUPAC (International Union of Pure and Applied Chemistry). The hysteresis presented in the isotherms was of type H1, which is characteristic of solid particles within cylindrical channels, with consolidated aggregates and agglomerates of spheroid particles. Based on the information from the isotherms and XRD patterns, the material's textural properties were determined and given in Table 1.

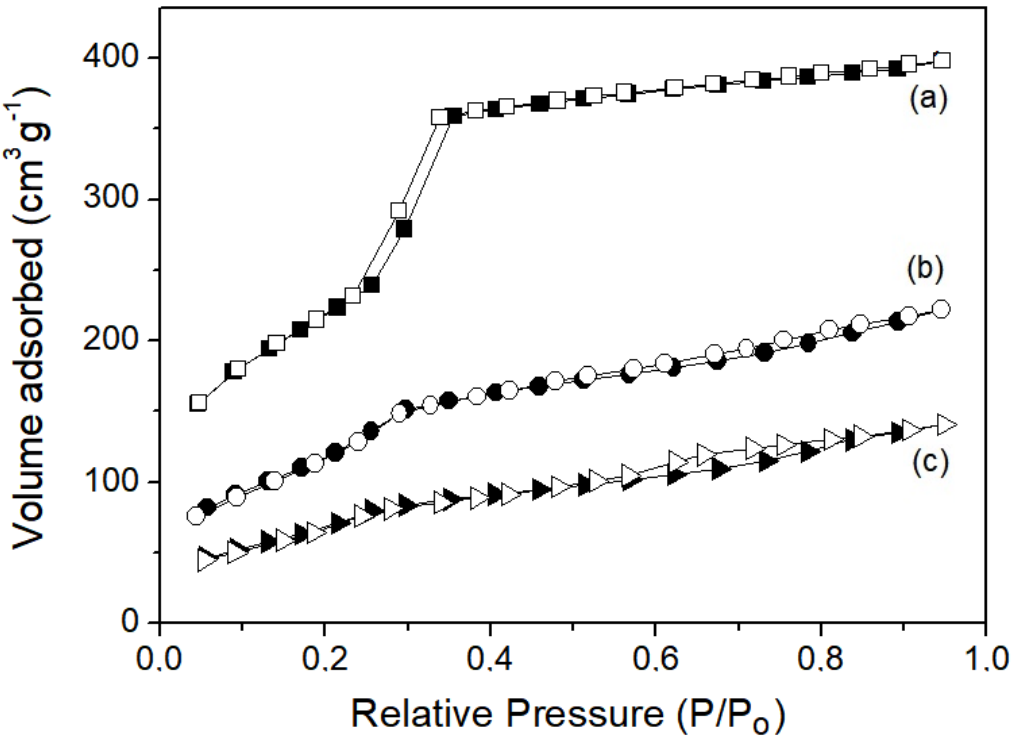

Figure 3 Isotherms Nitrogen adsorption-desorption of calcined materials: (a) MCM-41; (b) 31% TiO_2/MCM-41; (c) 48%TiO_2/MCM-41.

Table 1 Textural properties of the MCM-41 and TiO_2/MCM-41 materials.

Nanostructured Material	Surface area (m^2 g^{-1})	Pore volume (cm^3 g^{-1})	$d_{(100)}$ (nm)	P_d (nm)	a_0 [(a)](nm)	Wt [(b)](nm)
MCM-41	951	0.10	3.88	2.6	4.48	1.88
31%TiO_2/MCM-41	486	0.14	3.43	2.7	3.96	1.26
48%TiO_2/MCM-41	276	0.08	3.67	2.0	4.24	2.24

(a) $a_0 = 2d_{100}/\sqrt{3}$; (b) Wt is Wall thickness, $Wt = a_0 - P_d$, where P_d is the pore diameter.

The characteristics of the isotherms observed suggest that as the percentage of titanium dioxide supported increases on the MCM-41 support, occur a decrease in the regularity of the mesopores, thus resulting in a decrease in the surface of the catalysts, due to the filling of mesopores. The unsupported MCM-41 has a surface area of the 951 m^2g^{-1}, but after impregnation of different percentages of titanium dioxide, was observed a decreasing in the specific surface area to 486 and 276 m^2g^{-1}, for 31% and 48% of TiO_2, respectively. In addition, the unit cell parameter, which was obtained from the value of the interplanar distance in the plane (100) of XRD, and the wall thickness, which takes into account the parameter of the unit cell and the pore diameter, indicates that the materials showed an expressive ordered structure of pore and the wall thickness.

The FTIR spectra of the mesoporous materials are shown in the Figure 4. Seven absorption bands were identified in the spectra, typical for porous nanostructured silicates, due to the presence of T-O bonds in the TO_4 tetrahedra (T = Si) and surface hydroxyl groups. The maxim peaks of the absorption bands are identified with numbers from 1 to 7 in the spectra.

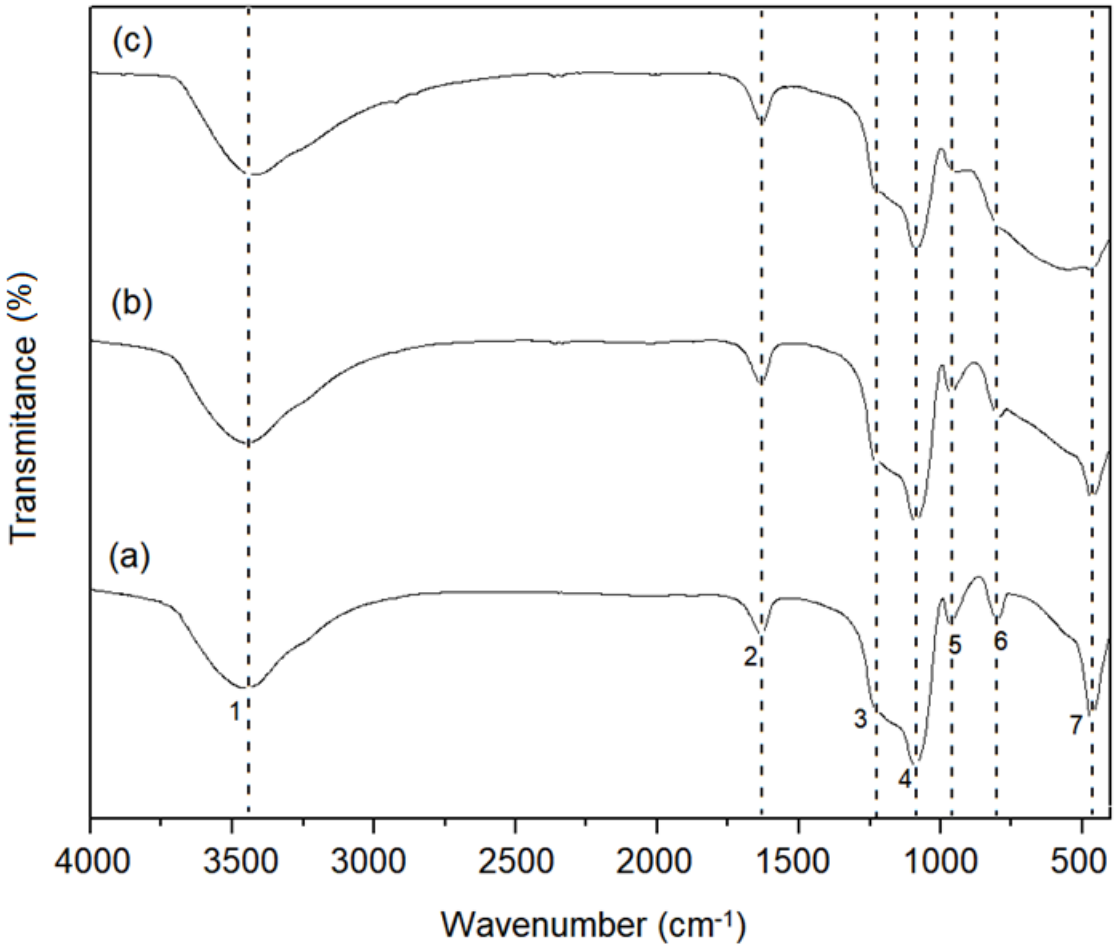

Figure 4 FTIR spectra of the mesoporous materials: (a) MCM-41; (b) 31%TiO_2/MCM-41 and (c) 48%TiO_2/MCM-41, showing infrared absorption bands of the materials.

The 3250-3750 cm^{-1} (peak 1) is related to hydroxyl groups inside and outside the mesoporous structure. The IR band at 1550-1750 cm^{-1} (peak 2) is attributed to the surface water. At region of 1240-1260 cm^{-1} (peak 3) is observed for the asymmetric stretching of Si-O and in the region of 1200-1100 cm^{-1} (peak 4) is assigned to vibrations of the Tetrahedrons T-O-T. The stretching bands in regions of 950 and 700 cm^{-1} (peaks 5 and 6) are assigned to the symmetrical links Si-O-Si and Si-O-M (M = Ti). The lower wavenumber is ascribed to the presence of tetrahedrally coordinated metal ions in the silica matrix. However, this band must be interpreted in terms of titanium overlay to what is seen by the increased intensity of the band when increasing the percentage of the titanium. The bands at 480-420 cm^{-1} (peak 7) are related to the asymmetric stretching of the TO bonds (T = Si, Ti) [41-45]. The presence of all absorption bands observed in Figure 4 is pieces of evidence that the hexagonal structure was maintained even after the impregnation of titanium oxide in the MCM-41 structure and subsequent calcination.

3.2 Catalytic Degradation of BTEX

The catalytic tests were carried out to evaluate the performance of the titanium-supported MCM-41 catalysts for oxidation of BTEX in the presence of hydrogen peroxide, varying the percentages of titanium dioxide. The obtained results showing the decreasing concentration of

benzene, toluene, ethylbenzene and xylenes, as a function of the reaction time, are presented in Figure 5.

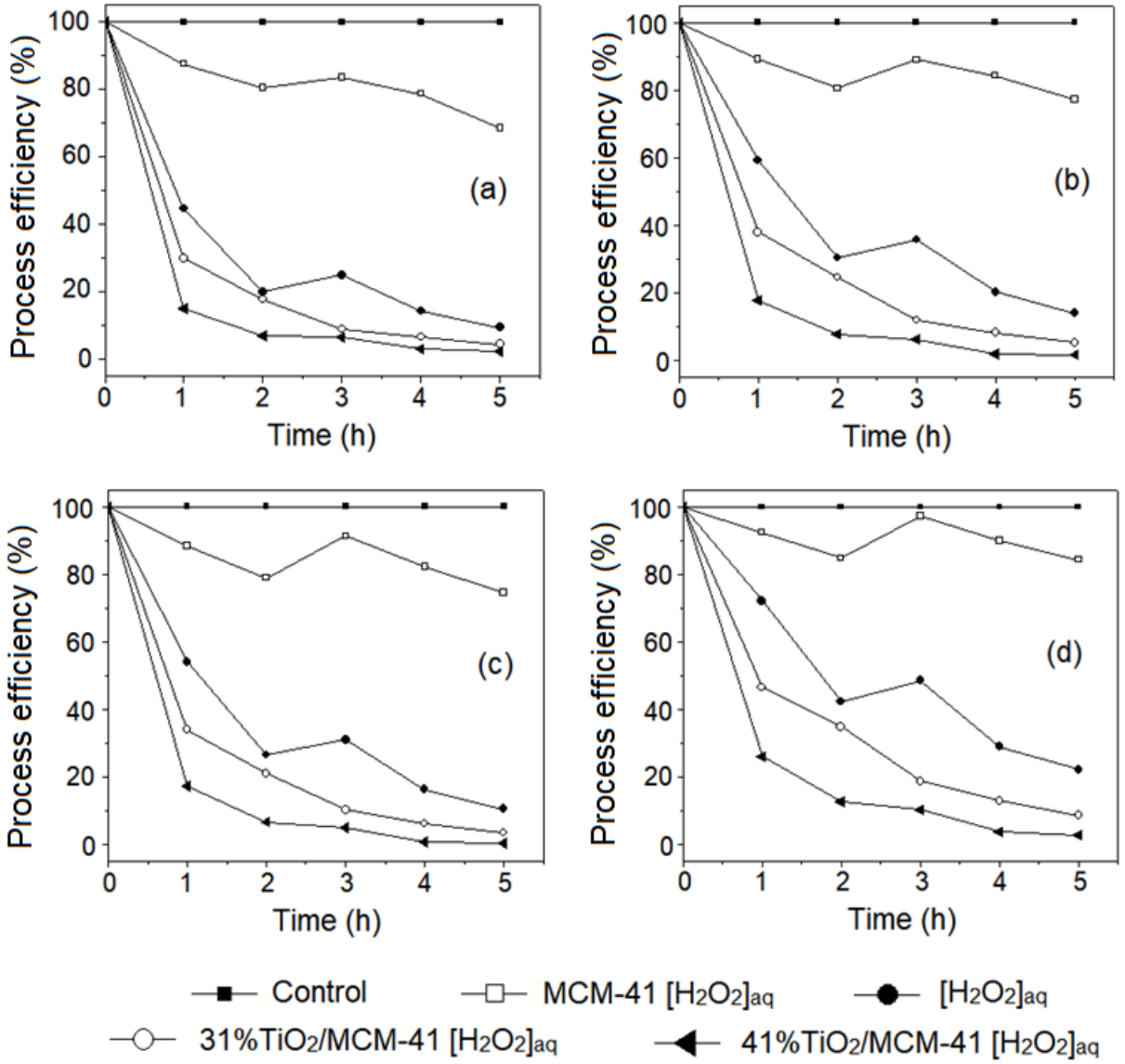

Figure 5 Catalytic performance of titanium supported MCM-41 catalysts for oxidation of organic compounds in aqueous media, in presence of hydrogen peroxide: (a) Benzene; (b) Toluene; (c) Ethylbenzene; (d) Xylenes.

According to the catalytic reactions, at 60°C no reaction was observed for the background BTEX (Control) in aqueous media, due to its stabilities at this temperature. However, it is proposed that in the presence of hydrogen peroxide, was observed some reactivity of the BTEX, due to the generation of hydroxyl radicals in aqueous media $[^{*}OH]_{aq}$ (eq. 02) that reacts directly with the aromatic compounds [ArH] occurring the oxidation of the aromatics $[ArH]_{ox}$ (eq. 03). For the TiO_2/MCM-41 catalysts, were observed high conversions, due to the hydroxyls generated from the reaction of titanium with hydrogen peroxide (eq. 04), that reacts with the aromatics [ArH], occurring the oxidation producing water (eq. 05). The hydroxyl radicals $[^{*}OH]$ react with hydrogen peroxide, producing more (eq. 06) and also reacts with the Ti^{3+}, regenerating the Ti^{4+} ions (eq. 07). (ArH =

Aromatic Hydrocarbon). All the equations represent speculative reactions occurring during the oxidation process.

$$H_2O_2 \rightarrow [^*OH]_{aq} + [^*OH]_{aq} \quad (2)$$

$$[^*OH] + ArH \rightarrow [ArH]_{OX} \quad (3)$$

$$Ti^{4+} + 2[^*OH] \rightarrow Ti^{3+} + H_2O_2 \quad (4)$$

$$ArH + [^*OH] \rightarrow [ArH]_{OX} + H_2O \quad (5)$$

$$[^*OH] + H_2O_2 \rightarrow H_2O + HO_2 \quad (6)$$

$$[^*OH] + Ti^{3+} \rightarrow Ti^{4+} + [^*OH] \quad (7)$$

In the presence of catalysts, the [*OH] radicals are formed from the interaction between the excited oxygen atom of the titanium oxide and the hydrogen atoms of the substrates cleaved or even hydrogen atoms from water, since the reactions occur in aqueous media [46, 47] as well as radicals derived from hydrogen peroxide, which increases the oxidation capability of the mesoporous materials. The subsequent oxidative reactions can transform the fragmented carbon dioxide and water. The effect of hydrogen peroxide was also observed for the degradation of benzene in water catalyzed by MCM-41 containing cobalt [48].

4. Conclusions

The impregnation method incorporated the titanium oxide into the MCM-41 nanomaterials, incorporating titanium in the mesoporous MCM-41 support. The techniques used to characterize these materials (XRD, nitrogen adsorption/desorption and FTIR) showed good results, demonstrating the maintenance of the hexagonal structure of the MCM-41, the efficiency of hydrothermal synthesis and the incorporation of titanium in the structure of the MCM-41. From the impregnation method and thermal treatment of the materials, the predominant anatase phase of the TiO_2 was obtained, which is the most active phase for oxidation reactions. The catalytic process of the BTEX compounds in the presence of hydrogen peroxide and titanium-supported mesoporous catalyst proved to be a highly effective material for hydrocarbon oxidation processes, in particular, organic compounds containing benzene rings. The TiO_2/MCM-41 materials showed a high catalytic activity due to the combination of hydrogen peroxide with the active phase of titanium supported on MCM-41, with oxidation conversions of about 95% of total oxidation. The high conversion results from combining H_2O_2 with titanium-based catalysts, in which the percentage of oxidation increases with the titanium loading in the mesoporous support. Thus, for 48%TiO_2/MCM-41 catalyst, a higher conversion of the BTEX was observed. This fact is related to the generation of hydroxyl radicals from the surface of the catalysts. Using the impregnation method with the evaporation of solvents, followed by thermal treatment, it was considered that the titanium had the maximum incorporation, with little or no possibility of leaching under the reaction conditions.

Acknowledgments

The authors thank the Brazilian Agency of Petroleum, Natural Gas and Biofules (ANP) and Nacional Concil of Research and Development (CNPq) for financial support.

Author Contributions

Dr. A.S.A and A.P.M.A.G. were responsible for project development, L.A.M, F.L.C. and M.F.F. conducted methodology and data collection, G.J.T.F. and V.J.F. analysis and investigation, M.D.S.A. writing and editing. All authors agreed to the published version of the manuscript.

Funding

The organization that funded this research was Nacional Council of Research and Development (CNPq, Process 306780/2018-6).

Competing Interests

The authors have declared that no competing interests exist.

References

1. Nakata K, Fujishima A. TiO_2 photocatalysis: Design and applications. J Photochem Photobiol C. 2012; 13: 169-189.
2. Schneider J, Matsuoka M, Takeuchi M, Zhang J, Horiuchi Y, Anpo M, et al. Understanding TiO_2 photocatalysis: Mechanisms and materials. Chem Rev. 2014; 114: 9919-9986.
3. Liu G, Yu JC, Lu GQ, Cheng HM. Crystal facet engineering of semiconductor photocatalysts: Motivations, advances and unique properties. Chem Commun. 2011; 47: 6763.
4. Ali I, Suhail M, Alothman ZA, Alwarthan A. Recent advances in syntheses, properties and applications of TiO_2 nanostructures. RSC Adv. 2018; 8: 30125-30147.
5. Fernández-Catalá J, Cazorla-Amorós D, Berenguer-Murcia Á. Facile encapsulation of P25 (TiO_2) in spherical silica with hierarchical porosity with enhanced photocatalytic properties for gasphase propene oxidation. Appl Catal A. 2018; 564: 123-132.
6. Kuwahara Y, Sumida Y, Fujiwara K, Yamashita H. Facile synthesis of yolk-shell nanostructured photocatalyst with improved adsorption properties and molecular-sieving properties. ChemCatChem. 2016; 8: 2781-2788.
7. Kuwahara Y, Yamashita H. Efficient photocatalytic degradation of organics diluted in water and air using TiO_2 designed with zeolites and mesoporous silica materials. J Mater Chem. 2011; 21: 2407-2416.
8. Jansson I, Suarez S, Garcia-Garcia FJ, Sanchez B. Zeolite-TiO_2 hybrid composites for pollutant degradation in gas phase. Appl Catal B. 2015; 178: 100-107.
9. Leary R, Westwood A. Carbonaceous nanomaterials for the enhancement of TiO_2 photocatalysis. Carbon. 2011; 49: 741-772.
10. Zhang W, Li G, Liu H, Chen J, Ma S, Wen M, et al. Photocatalytic degradation mechanism of gaseous styrene over Au/TiO_2@ CNTs: Relevance of superficial state with deactivation mechanism. Appl Catal B. 2020; 272: 118969.

11. Padervand M. Reusable porous $Na(SiAl)O_6.xH_2O/NiFe_2O_4$ structure for selective removal of heavy metals from waste waters. Hong Kong: IFI CLAIMS Patent Services; 2021; United States patent US 11,014,082.
12. Mohsen P, Shahnaz G, Sima H, Baker R, Zahra GN, Saeed K, et al. Multifunctional $Ag/AgCl/ZnTiO_3$ structures as highly efficient photocatalysts for the removal of nitrophenols, CO_2 photoreduction, biomedical waste treatment, and bacteria inactivation. Appl Catal A. 2022; 643: 118794.
13. Mohsen P, Farnaz A, Ali A, Bagher ES, Gerhard L. Hexagonal core-shell SiO_2[–MOYI]Cl–]Ag nanoframeworks for efficient photodegradation of the environmental pollutants and pathogenic bacteria. J Inorg Organomet Polym Mater. 2019; 29: 1314-1323.
14. Mohsen P, Sima H. Ag/AgCl@Tubular g-C_3N_4 nanostructure as an enhanced visible light photocatalyst for the removal of organic dye compounds and biomedical waste under visible light. J Photochem Photobiol A. 2022; 425: 113700.
15. Mohsen P, Farideh N, Sima H, Alireza B, Sheida E, Mojtaba A, et al. $Ag@Ag_2MoO_4$ decorated polyoxomolybdate/C_3N_4 nanostructures as highly efficient photocatalysts for the wastewater treatment and cancer cells killing under visible light. Inorg Chem Commun. 2022; 141: 109500.
16. Mohsen P, Gerhard L, Alireza B, Hamid MS. Photochemical degradation of the environmental pollutants over the worm-like Nd_2CuO_4-Nd_2O_3 nanostructures. Nano-Struct Nano-Objects. 2019; 18: 100258.
17. Mohsen P, Shahnaz G, Sima H, Chuanyi W. $K_4Nb_6O_{17}/Fe_3N/\alpha$-$Fe_2O_3/C_3N_4$ as an enhanced visible light-driven quaternary photocatalyst for acetamiprid photodegradation, CO_2 reduction, and cancer cells treatment. Appl Surf Sci. 2021; 544: 148939.
18. Lovanh N, Hung CS, Alvarez PJJ. Effect of ethanol on BTEX biodegradation kinetics: Aerobic continuous culture experiments. Water Res. 2002; 36: 3739-3746.
19. Xin BP, Wu CH, Lin CW. Bioaugmented remediation of high concentration BTEX-contaminated groundwater by permeable reactive barrier with immobilized bead. J Hazard Mater. 2013; 244-245: 765-772.
20. Wu H, Wang L, Zhang J, Shen Z, Zhao J. Catalytic oxidation of benzene, toluene and *p*-xylene over colloidal gold supported on zinc oxide catalyst. Catal Commun. 2011; 12: 859-865.
21. Do SH, Kwon YJ, Klong SH. Feasibility study on an oxidant-injected permeable reactive barrier to treat *BTEX* contamination: Adsorptive and catalytic characteristics of waste-reclaimed adsorbent. J Hazard Mater. 2011; 191: 19-25.
22. LaoKiat L, Khemthong P, Grisdanurak N, Sreearunothai P, Pattanasiriwisawa W, Klysubun W. Photocatalytic degradation of benzene, toluene, ethylbenzene, and xylene (BTEX) using transition metal-doped titanium dioxide immobilized on fiberglass cloth. J Chem Eng. 2012; 29: 377-383.
23. Britto JM, Rangel MC. Processos avançados de oxidação de compostos fenólicos em efluentes industriais. Quim Nova. 2008; 31: 114-122.
24. Segura Y, Martínez F, Melero JA, Molina R, Chand R, Bremner DH. Enhancement of the advanced Fenton process (Fe^0/H_2O_2) by ultrasound for the mineralization of phenol. Appl Catal B. 2012; 113: 100-106.
25. Petrova P, Tabakova T, Munteanu G, Zanella R, Tsvetkov M, Ilieva L. Gold catalysts on Co-doped ceria for complete benzene oxidation: Relationship between reducibility and catalytic activity. Catal Commun. 2013; 36: 84-88.

26. Beck JS, Vartuli JC, Roth WJ, Leonowicz ME, Kresge CT, Schmitt KD, et al. A new family of mesoporous molecular sieves prepared with liquid crystal templates. J Am Chem Soc. 1992; 114: 10834-10843.
27. Can M, Akça B, Yilmaz A, Üner D. Synthesis and characterization of Co-Pb/SBA-15 mesoporous catalysts. Turkish J Phys. 2005; 29: 287-293.
28. Wu Y, Zhang Y, Cheng J, Li Z, Wang H, Sun Q, et al. Synthesis, characterization and catalytic activity of binary metallic titanium and iron containing mesoporous silica. Microporous Mesoporous Mater. 2012; 162: 51-59.
29. Chen L, Liu F, Liu Y, Dong H, Colberg PJS. Benzene and toluene biodegradation down gradient of a zero-valent iron permeable reactive barrier. J Hazard Mater. 2011; 188: 110-115.
30. Chen YW, Lin HY. Characteristics of Ti-MCM-41 and its catalytic properties in oxidation of benzene. J Porous Mater. 2002; 9: 175-184.
31. Popova M, Szegede A, Kostova N, Tsoncheva T. Titanium modified MCM-41 as a catalyst for toluene oxidation. Catal Commun. 2008; 10: 304-308.
32. Rios LA, Weckes P, Schuster H, Hoelderich WF. Mesoporous and amorphous Ti–silicas on the epoxidation of vegetable oils. J Catal. 2005; 232: 19-26.
33. Berlini C, Guidotti M, Moretti G, Psaro R, Ravasio N. Catalytic epoxidation of unsaturated alcohols on Ti-MCM-41. Catal Today. 2000; 60: 219-225.
34. Araujo AS, Aquino JMFB, Souza MJB, Silva AOS. Synthesis, characterization and catalytic application of cerium-modified MCM-41. J Solid State Chem 2003; 171: 371-374.
35. Souza MJB, Araujo AS, Pedrosa AMG, Marinkovic BA, Jardim PM, Morgado E. Textural features of highly ordered Al-MCM-41 molecular sieve studied by X-ray diffraction, nitrogen adsorption and transmission electron microscopy. Mater Lett. 2006; 60: 2682-2685.
36. Antochshuk V, Araujo AS, Jaroniec M. Functionalized MCM-41 and CeMCM-41 materials synthesized via interfacial reactions. J Phys Chem B. 2000; 104: 9713-9719.
37. Fernandes GJT, Coriolano AC, Silva JB, Castro FL, Fernandes VJ, Araujo AS. Synthesis characterization and acid properties of niobium-containing MCM-41. J Therm Anal Calorim. 2017; 131: 691-695.
38. Adan C, Carbajo J, Bahamonde A, Oller I, Malato S, Martinez-Arias A. Solar light assisted photodegradation of phenol with hydrogen peroxide over iron-doped titania catalysts: Role of iron leached/readsorbed species. Appl Catal B. 2011; 108: 168-176.
39. McManamon C, Holmes JD, Morris MA. Improved photocatalytic degradation rates of phenol achieved using novel porous ZrO_2-doped TiO_2 nanoparticulate powders. J Hazard Mater. 2011; 193: 120-127.
40. Matsumoto D, Diniz LA, Castro LS, Teixeira ACSC, Guardani R, Paiva JL. Kinetic modeling and experimental validation of a photocatalytic fluidized bed reactor for *n*-hexane degradation. Braz J Chem Eng. 2019; 36: 1561-1570.
41. Calabro DC, Valyocik EW, Ryan FX. In situ ATR/FTIR study of mesoporous silicate syntheses. Microporous Mater. 1996; 7: 243-259.
42. Zholobenko VL, Holmes SM, Cundy CS, Dwyer J. Synthesis of MCM-41 materials: An in situ FTIR study. Microporous Mater. 1997; 11: 83-86.
43. Thanabodeekij N, Tanglumlert W, Gulari E, Wongkasemjit S. Synthesis of Ti-MCM-41 directly from silatrane and titanium glycolate and its catalytic activity. Appl Organomet Chem. 2005; 19: 1047-1054.

44. Orlov A, Zhal QZ, Klinowski J. Photocatalytic properties of the SBA-15 mesoporous silica molecular sieve modified with titanium. J Mater Sci. 2006; 41: 2187-2193.
45. Popova M, Szegedi A, Cherkezova-Zheleva Z, Mitov I, Kostova N, Tsoncheva T. Toluene oxidation on titanium- and iron-modified MCM-41 materials. J Hazard Mater. 2009; 168: 226-232.
46. Chaliha S, Bhattacharyya KG. Fe(III)-, Co(II)- and Ni(II)-impregnated MCM41 for wet oxidative destruction of 2,4-dichlorophenol in water. Catal Today. 2009; 141: 225-233.
47. Stovanova M, Christoskova ST, Georgieva M. Mixed Ni-Mn-oxide systems as catalysts for complete oxidation: Part II. Kinetic study of liquid-phase oxidation of phenol. Appl Catal A. 2003; 249: 295-302.
48. Farias MF, Domingos YS, Fernandes GJT, Castro FL, Fernandes Jr VJ, Costa MJF, Araujo AS. Effect of acidity in the removal-degradation of benzene in water catalyzed by Co-MCM-41 in medium containing hydrogen peroxide. Microporous Mesoporous Mater. 2018; 258: 33-40.